www.nature.com/scientificreports

scientific reports

OPEN

Imperfect hydroxyapatite bioceramics derived from golden pomfret have enhanced osteogenic properties

Changze Zhang[1,4,5], Guangchun Zhao[1,4,5], Xiaorui Wang[1], Mengting Li[1]✉, Zhengmao Li[3], Yixun E[1], Xiaxin Cao[1], Maohua Chen[2]✉ & Chaozong Liu[4]✉

Imperfect hydroxyapatite (IHA) bioceramics, which contain defects such as calcium deficiency, carbonate substitution, and metal cation substitution, exhibit improved osteogenic properties. In this study, we used a two-step calcination-hydrothermal process to manufacture two types of golden pomfret bone-derived imperfect hydroxyapatite bioceramics (G-IHA): carbonated calcium-deficient hydroxyapatite (CD-IHA) and carbonated hydroxyapatite (C-IHA). Their composition, surface morphology, zeta potential, degradation capacity, mineralization and osteogenic properties were systematically investigated. The results revealed that G-IHA with a higher defect content, including A-type carbonate substitution and Ca vacancies, had negatively charged surface. As a result, G-IHA surfaces are more favourable to ion exchange and interaction with cations (e.g., Na^+, Ca^{2+}) in the microenvironment, which results in improved degradation and mineralization. Specifically, after 28 days of degradation, G-IHA showed significantly higher weight losses (CD-IHA and C-IHA were 17% and 13%, respectively) than commercial hydroxyapatite (CHA; 7%). In addition, G-IHA have a higher better bone-like apatite formation ability, and a higher degree of osteogenic differentiation than CHA. Notably, carbonated calcium-deficient imperfect hydroxyapatite (CD-IHA) exhibited the highest bioactivity and osteogenic capacity as evidenced by its increased alkaline phosphatase activity and improved bone matrix mineralization capacity. In conclusion, this study revealed that imperfect hydroxyapatite bioceramics derived from golden pomfret bone have the potential to enhance osteogenic properties and be employed in clinical settings as bone substitute materials.

Keywords Calcium-deficient hydroxyapatite, Carbonate substitution hydroxyapatite, Cation exchange, Enhanced osteogenic property, Golden pomfret bone

The Global Burden of Diseases, Injuries, and Risk Factors Study indicated that the number of prevalent cases of acute or long-term symptoms of a fracture had reached 455 million by 2019, representing a 70.1% increase compared with 1990[1]. Although bone tissue can regenerate to some extent, when bone deficiencies are larger than the critical size and are induced by external sources, including fractures, bioactive bone transplants are required to promote bone regeneration[2]. Hydroxyapatite ($Ca_{10}(PO_4)_6(OH)_2$), a calcium phosphate (CaP) compound, has been extensively employed as a bone transplant material because of its superior osteoinductive activity[3]. The majority of hydroxyapatite found in natural bone is calcium-deficient ($Ca_{10-x}(HPO_4)_x(PO_4)_{6-x}(OH)_{2-x}$, $0 < x < 1$, CDHA)[4];[5].

Compared with HA, CDHA, whose amorphous surface layer provides a metastable non-apatite environment, promotes ion exchange on its surface, resulting in superior bioactivity[6–8]. Zhang et al. investigated the effects of HA and CDHA on mouse bone mesenchymal stem cells (BMSCs). The results indicated that CDHA exhibited more favourable effects than HA in terms of cell proliferation, alkaline phosphatase activity, and expression

[1]School of Chemistry and Chemical Engineering, Hainan University, Haikou 570228, China. [2]Laboratory of Digital Medical Engineering, Key Laboratory of Biomedical Engineering of Hainan Province, School of Biomedical Engineering, Hainan University, Sanya 572025, China. [3]School and Hospital of Stomatology, Guangzhou Medical University, Guangzhou 510182, China. [4]Institute of Orthopaedic & Musculoskeletal Science, University College London, Royal National Orthopaedic Hospital, London HA74LP, UK. [5]Changze Zhang and Guangchun Zhao contributed equally to this work. ✉email: limengting@hainanu.edu.cn; maohuachen@hainanu.edu.cn; chaozong.liu@ucl.ac.uk

of osteogenesis-related genes[9]. After evaluating the osteogenic potential of HA and CDHA in vivo, Bulina et al. observed that CDHA exhibited almost complete remodelling of injured rat bone tissue after just 5 months, whereas HA only showed partial remodelling[10].

Compared to pure HA, carbonated HA, which facilitates the release of BMP6 and Wnt10b, can promote osteoblastic differentiation[11–13]endowing carbonated HA with superior osteogenic activity. Fish bones are an excellent source of carbonated hydroxyapatite for bone graft materials[14];[15]. Shi et al. demonstrated that carbonated hydroxyapatite originating from rainbow trout or salmon bones can enhance mouse pre-osteoblast MC3T3-E1 proliferation and differentiation[16]. Deng et al. found that carbonated biphasic CaP derived from butterfish bones possesses superior biocompatibility and osteogenic potential in vivo and in vitro[17].

The golden pomfret fish (Trachinotus ovatus) is cultivated in China, Singapore, and Malaysia[18]. The annual production of golden pomfret in southern China is 120 thousand tons[19]. However, research on golden pomfret has been mainly focused on its cultivation or processing for food[20–22]. Bone-derived biomaterials have received little attention.

In this study, golden pomfret bone was used to generate two types of imperfect hydroxyapatites, carbonated calcium-deficient imperfect hydroxyapatite (CD-IHA) and carbonated imperfect hydroxyapatite (C-IHA), through a two-stage hydrothermal calcination process. Initially, the phase composition, crystal structure, surface charge properties, mineralization capacity, and degradation rates of the CD-IHA, C-IHA and CHA bioceramic samples were investigated to characterize the properties of the bioceramics derived from golden pomfret bone. Subsequently, the in vitro biological performance of the bioceramic samples was evaluated to confirm their osteogenic performance and biomaterial applications, including phosphate buffered saline (PBS) buffer immersion, bone-like apatite formation, cell viability, and osteoblastic differentiation of BMSCs.

Materials and methods

Materials

The raw material used in this study was golden pomfret purchased from Hainan Xiangtai Fishery Company Limited, Chengmai, Hainan Province, China. As a control, CHA was obtained from Wuhan Lullaby Pharmaceutical Chemical Company, Ltd. (Wuhan, Hubei Province, China). Furthermore, the simulated body fluid (SBF) solution was prepared as described by Oyane et al.[23]but at double the concentration.

Preparation of imperfect hydroxyapatite bioceramics derived from golden pomfret

The golden pomfret bones were calcined at 800 °C for 6 h in an air atmosphere and subjected to ball milling for 12 h. Subsequently, the ball-milled bones were mixed with ammonium phosphate dibasic ($(NH_4)_2HPO_4$) at a mass ratio of 1:1 and added in deionized water, maintaining at 160 °C for 3 h to obtain CD-IHA. When the temperature of calcination was elevated to 600 °C, C-IHA was obtained (Fig. 1).

Characterization

The phases of the samples were analyzed by X-ray diffraction (XRD) analyzer (Smart Lab, Rigaku, Japan) using Cu Kα1 radiation at 40 kV in the 2θ range of 10-80°, and the crystal structure data was calculated by Rietveld method for lattice parameters calculation[24]. The crystallinity was calculated according to Alain Person's research[25]. For composition characterization, a Fourier-transform infrared (FTIR) spectrometer (T27, Bruker, Germany) was used in the range of 4000–400 cm^{-1}. Derivative thermogravimetry (DTG) graphs of the samples were recorded using thermogravimetric analysis (TGA) data. The analyses were carried out on a thermogravimetric analyzer (STA449F5, Netzsch, Germany) at 25–1100 °C with a heating rate of 10 °C/min. An energy dispersive spectrometer (EDS) attached to a scanning electron microscope (SEM) at 3 kV was used for morphological and elemental analyzes. The surface charge of the samples was measured using a zeta potential analyzer (Zetasizer Nano ZS90, Malvern Instruments, Britain) at a suspension concentration of 12.5 mg/mL.

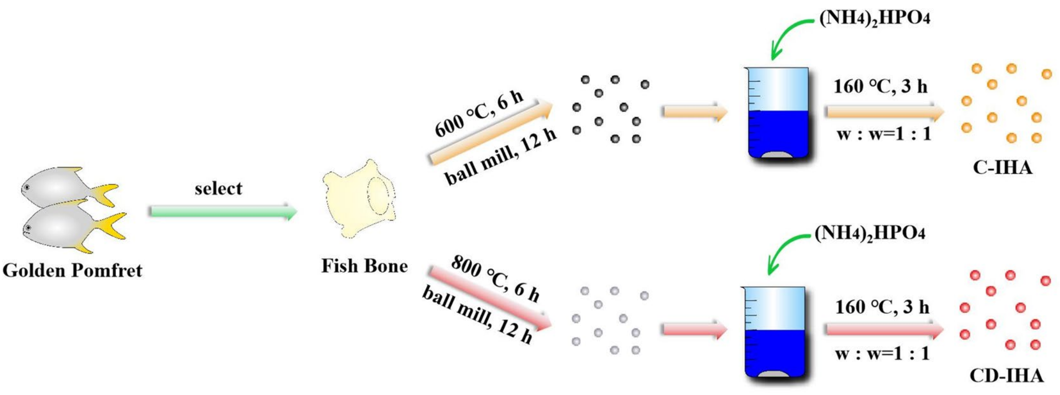

Fig. 1. Process of preparing bioceramics derived from golden pomfret.

In vitro studies

Degradation

Samples were immersed in PBS to be oscillated at 37 °C for 7, 14, 21 and 28 days at a concentration of 1 mg/mL each. Each suspension was centrifuged for 1 min at 6577 x g. Finally, the pH of the supernatant was analyzed, and the mass of precipitate that had been dried at 60 °C was quantified. Each experiment was conducted in triplicate.

About degradation rate, the weight loss (%) was calculated by the Eq. (1):

$$\mathrm{w}(\%)=\frac{\mathrm{m_0}-\mathrm{m}}{\mathrm{m_0}}\times 100\% \tag{1}$$

Where, w is the degradation rate of the sample, m_0 is the initial mass of the sample, and m is the mass of the corresponding precipitate.

Mineralization

Each sample was immersed in SBF and oscillated at 37 °C at a concentration of 1 mg/mL. The SBF was updated every 7 days to ensure an adequate ionic concentration for mineral nucleation and growth. After 14-days of immersion, the precipitate was separated and dried at 60 °C. The composition and morphology of the precipitate was analyzed by XRD, FTIR and SEM by the method in section "Characterization" of this article.

Cytocompatibility

The L929 fibroblasts were cultured with a medium (RPMI-1640 supplemented with 10% fetal bovine serum and 1% penicillin-streptomycin mixture) containing various concentrations of samples (0 µg/mL (control), 400 µg/mL, 600 µg/mL, 800 µg/mL and 1000 µg/mL) for 24 h. The BMSCs were cultured under the same conditions, except that the medium was mainly DMEM-F12 instead. Subsequently, cell viability was measured by replacing the complete medium with 100 µL/mL cell counting kit-8 reagent (CCK-8; Dojindo, Japan) and culturing for another 1 h. The optical density (OD) of each well was analyzed using a microplate reader (Synergy LX, Biotek, USA) at 450 nm. The survival of the cells co-cultured with the samples was calculated according to Eq. (2) [26]:

$$\mathrm{Sur}(\%)=\frac{\mathrm{A_s}-\mathrm{A_0}}{\mathrm{A_c}-\mathrm{A_0}}\times 100\% \tag{2}$$

where Sur represents the survival of cells cultured with samples, A_s represents the OD of wells with the sample, A_c represents the OD of the control, and A_0 represents the OD of the blank. A blank group was established using the corresponding complete medium without cells.

At the same time, cell proliferation was further evaluated by live/dead staining. Briefly, the cultured wells were stained using calcein-AM/PI kit (Sigma Aldrich, USA) for 30 min and imaged under a microscope.

Osteogenic ability

The osteogenic ability of the samples was assayed using alkaline phosphatase (ALP) and Alizarin red S (ARS) staining. For ALP or ARS staining, BMSCs were co-cultured with 1 mg/mL samples by the method described in section "Cytocompatibility" for 7 or 14 days, respectively. Subsequently, each well was fixed with 4% paraformaldehyde (Service Bio, China) and cultured with a BCIP/NBT ALP colour development kit (Beyotime, China) or ARS solution (OriCell, China) at about 25 °C for 30–10 min, respectively. Thereafter, the cells were imaged under a microscope. The ALP- and ARS-stained areas were calculated to quantify their corresponding activities[27–29] using Python 3.11.

Statistical analysis

In this study, Microsoft Excel 2019 was employed to conduct pairwise F-tests and t-tests on the data. Specifically, when $p > 0.05$, a heteroscedasticity t-test was performed on the paired data. Conversely, when $p < 0.05$, a homoscedasticity t-test was conducted on the paired data using the F-test. Statistically significant differences between the two groups are indicated by * ($p < 0.05$), ** ($p < 0.01$), or *** ($p < 0.001$) in the t-test.

Results and discussion

Composition

Golden pomfret bone-derived imperfect hydroxyapatite bioceramics (G-IHA) were prepared using a two-step calcination-hydrothermal method. About the crystal phase, XRD peaks at 32.0°, 32.4°, and 33.1°, which were individually identified as the (211), (112) and (300) reflections of HA (ICDD PDF No. 09-0432)[30]were observed for both G-IHA and CHA (Fig. 2.a). G-IHA prepared by calcining golden pomfret exhibits a higher crystallinity (~ 85%; Table 1).

Furthermore, the Ca/P ratio of CD-IHA was determined to be 1.33, which is lower than that of standard hydroxyapatite (HA), carbonate-hydroxyapatite (CHA), and carbonated hydroxyapatite (C-IHA), with values of 1.67, 1.55, and 1.76, respectively (Fig. 2.b). As for previous research, when the Ca/P ratio approaches 1.4, calcium vacancies are formed within the hydroxyapatite lattice[31]. This finding provides additional evidence for the presence of calcium vacancies in CD-IHA. Conversely, C-IHA does not display any calcium vacancies in its structure, a difference that can be attributed to the distinct calcination temperatures employed during their synthesis.

Due to the lower sintering temperature of C-IHA, there are no obvious calcium vacancies in its structure. As shown in Fig. 2.c, metallic vacancy formation energy (ΔE) in materials is negatively correlated with calcination temperature at constant thermodynamic conditions, including the boiling point, molar heat of evaporation,

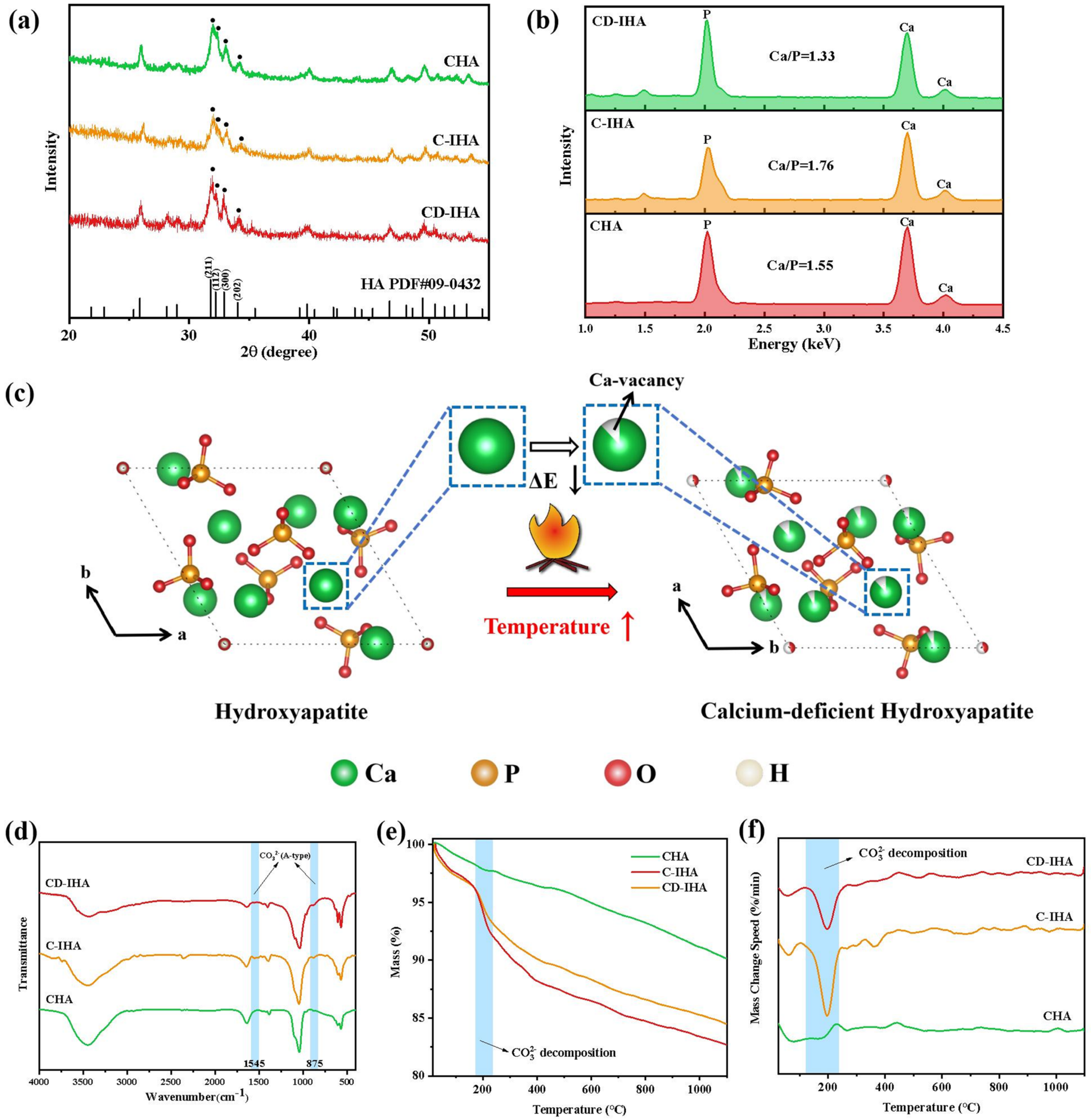

Fig. 2. (a) XRD pattern of CHA, C-IHA and CD-IHA; (b) EDS spectra and the calculated Ca/P ratio of CHA, C-IHA and CD-IHA ; (c) Mechanism of calcium vacancy formation in the HA structure above 800 °C (analyzed by VESTA software[69]); (d) FTIR spectra of CHA, C-IHA, and CD-IHA; (e) TG graphs of CHA, C-IHA, and CD-IHA; and (f) DTG graphs of CHA, C-IHA, and CD-IHA calculated by TG data.

Samples	a (Å)	c (Å)	Crystallinity (%)
Standard HA	9.418	6.884	-
CHA	9.394	6.885	58.64
C-IHA	9.416	6.893	85.12
CD-IHA	9.421	6.878	88.91

Table 1. Crystal structure data of the standard HA and samples.

specific heat at constant volume and temperature profiles[32]. Therefore, the higher the calcination temperature of the same material, the easier the formation of metallic vacancies.

The FTIR spectra of G-IHA exhibited two absorption bands at 875 cm^{-1} and 1545 cm^{-1} (Fig. 2.d). These bands are attributed to A-type carbonate substitution in the apatite structure, where the hydroxyl group (OH^-) was replaced by carbonate ions[33]. The obtained results were consistent with previous findings[34–36]. TG and DTG analysis were conducted to further investigate the carbonate substitution in G-IHA. In comparison to CHA, a distinct weight loss was observed in G-IHA at approximately 200 °C in G-IHA (Fig. 2.e and 2.f). This is attributed to the generation of CO_2 in carbonated HA at roughly 200 °C[37]. According to previous research, the reactions can be described by the Eqs. (3) and (4)[38,39].

$$CO_3^{2-} + H_2O \rightarrow HCO_3^- + OH^- \tag{3}$$

$$HCO_3^- \rightarrow CO_2 \uparrow + OH^- \tag{4}$$

Therefore, G-IHA was successfully prepared through calcination at 600 °C or 800 °C with subsequent hydrothermal treatment. Both were carbonated, with CD-IHA, possessing Ca vacancies.

Surface charge

A negatively charged surface promotes the deposition of apatite and enhances the adhesion of pre-osteoblasts, thereby facilitating bone mineralization and osteoblastic differentiation[40,41]. As a result, the surface charges of the samples were determined by their zeta potentials[42]. The results in Fig. 3.a showed that zeta potentials of CHA, C-IHA and CD-IHA are − 0.03 mV, − 14.03 mV and − 37.50 mV, respectively. This suggested that the surfaces of G-IHA were negatively charged, while the surfaces of CD-IHA had more of negative charges than the surfaces of C-IHA. The phenomenon may be attributed to the carbonate substitution of imperfect hydroxyapatite, which elevates the concentration of negatively charged groups on the C-IHA surface[43]. In the meantime, the negative charges will be increased by an abundance of Ca vacancies in the CD-IHA[44,45].

Consequently, G-IHA exhibited a negative charge due to carbonate substitution as well as calcium vacancies inside its lattice structure. (Fig. 3.b).

In vitro degradation

Degradation performance is a key indicator in the evaluation of bone grafts[2]. Therefore, the degradation rates of CHA and golden pomfret bone-derived imperfect hydroxyapatite bioceramics (G-IHA) were evaluated in PBS for 28 days. After 28 days of immersion, the degradation rates of CD-IHA, C-IHA and CHA reached 17%, 13% and 7%, respectively (Fig. 4.a). Although G-IHA has higher crystallinity than CHA as reported in Table 1, its degradation rate is accelerated due to crystal defects and carbonate substitution.

The degradation of G-IHA is significantly influenced by the ion exchange process of cations across the degradation zone[46]. The cations in PBS, primarily Na^+ and K^+, can be readily absorbed by the negatively charged G-IHA[47]. Subsequently, the anions on the G-IHAs interact with these cations, resulting in the formation of soluble salts (sodium or potassium salt) that dissolve in PBS solution and promote a loss of mass in the G-IHAs (Fig. 4.b). Furthermore, the crystal defects in G-IHA, resulting in irregular grain boundaries, also accelerate their degradation[48,49]. Simultaneously, the amorphous surface layer of CD-IHA, which facilitates ion exchanges via the metastable non-apatite surface, may further enhance the degradation rate[6–8]. Therefore, CD-IHA with higher negative charges exhibited improved degradation properties as compared to the C-IHA and CHA ($*p < 0.05$). (Fig. 4.a and b).

In addition, during the degradation process of all samples, the pH of the corresponding samples was maintained within the range of 7.15–7.55 (Fig. 4.c), which is similar to the pH observed in the environment of the human bone[50].

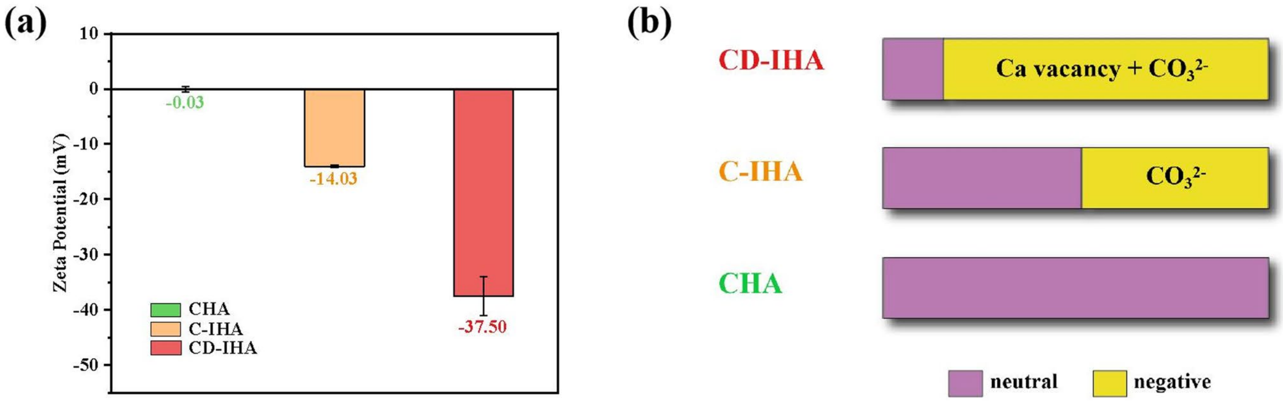

Fig. 3. (a) Zeta potentials of CHA, C-IHA and CD-IHA; and (b) sources of charges in CHA, C-IHA and CD-IHA.

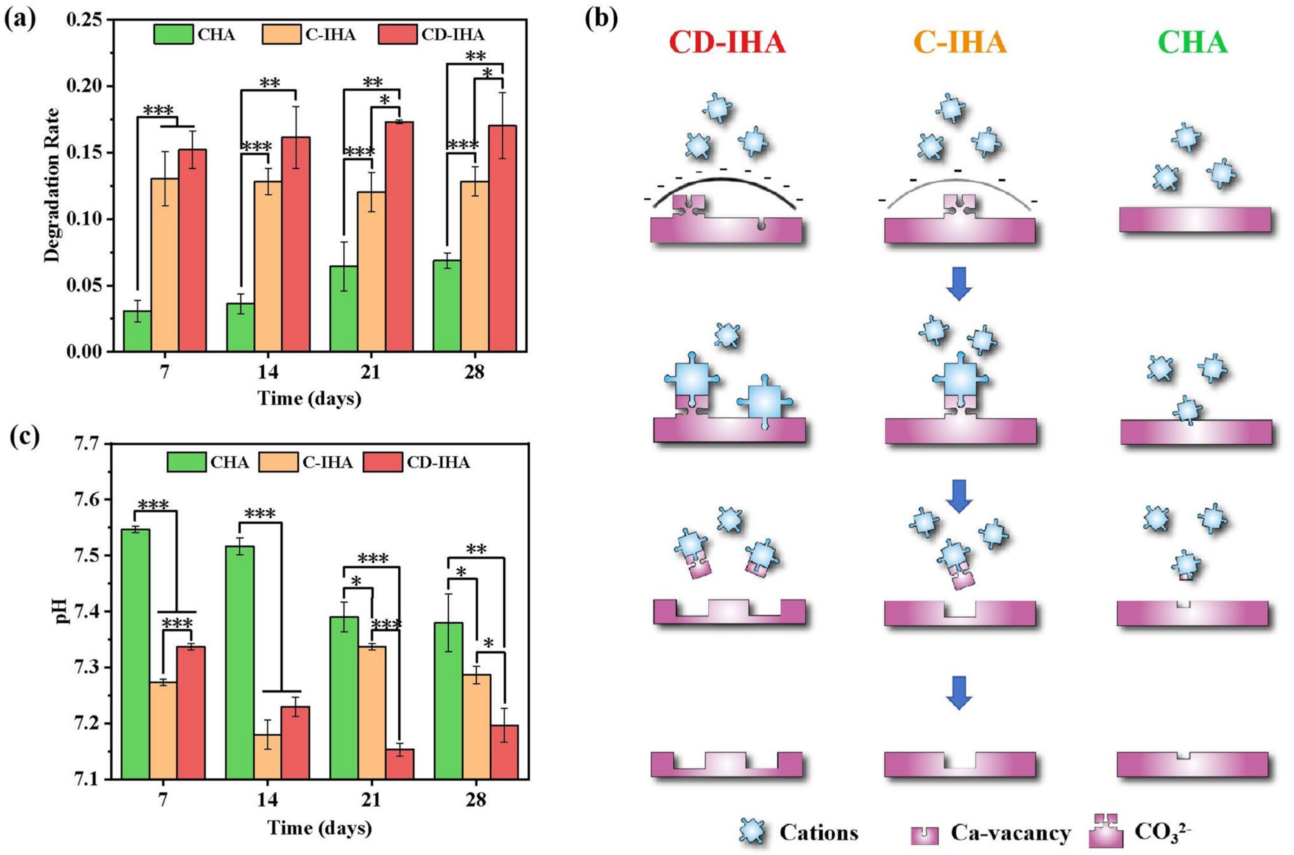

Fig. 4. (a) Degradation rate of CHA, C-IHA, and CD-IHA in vitro; (b) degradation mechanism of CHA, C-IHA, and CD-IHA in vitro; and (c) pH variation during the degradation of CHA, C-IHA, and CD-IHA in vitro.

In vitro mineralization

Mineralization test in vitro is capable of identifying the reliably osteoinductive materials[51]. Therefore, it is important to evaluate the in vitro mineralization properties of bone grafts.

XRD results indicated that both CHA and golden pomfret bone-derived imperfect hydroxyapatite bioceramics (G-IHA) had an increase in major peak intensity and a decrease in half-weight width after 14 days of immersion in SBF (Fig. 5.a). This is a result of the deposition of new apatite on the surface of both samples[52,53]. Furthermore, new peaks appeared in both immersed CHA and G-IHA at 27.4° (Fig. 5.a), which could be attributed to the (002) reflection of the deposited carbonate hydroxyapatite[54]. According to previous studies, the peak at 46° corresponds to the (221) reflections of aragonite commonly formed by Ca^{2+} and CO_3^{2-} in SBF[55].

Moreover, SEM results (Fig. 5.b) showed that the morphology of immersed G-IHA transferred into flower-like, indicating that G-IHA had apatite deposited on its surface. In addition, a new band at 1409 cm^{-1} appeared in the FTIR spectra of immersed samples (Fig. 5.c), suggesting that CO_3^{2-} substituted PO_4^{3-} and B-type CO_3^{2-} developed in their deposited apatite structure[56,57]. The B-type CO_3^{2-} is predominant form of CO_3^{2-} in human bone[58]suggesting that the deposition on the samples appeared like bone-like apatite. Notably, CD-IHA exhibited a stronger band than C-IHA and CHA (Fig. 5.c), suggesting enhanced deposition of bone-like apatite on CD-IHA.

The process of mineralization is associated with ion interaction[47]. In a manner similar to degradation, the negatively charged surface with apatite structure, having high binding affinity, preferentially attracts cations (such as Ca^{2+}) from SBF solution. As a consequence, the calcium-rich surface attracts PO_4^{3-} from the SBF, resulting in a cation-deficient surface that has the potential to continue attracting Ca^{2+}[40]. Being negatively charged, G-IHA perform superior mineralization properties than CHA. Furthermore, since CD-IHA takes advantage of ion interaction more than C-IHA[6–8]more Ca^{2+} and PO_4^{3-} ions are attracted to develop a new layer of apatite[40]resulting in enhanced mineralization properties (Fig. 5.d). Overall, CD-IHA demonstrated superior mineralization properties compared to other bioceramics.

Cytocompatibility

Cytocompatibility is an important consideration in bone-tissue engineering[59]. Therefore, we evaluated the cytocompatibility of CHA and golden pomfret bone-derived imperfect hydroxyapatite bioceramics (G-IHA). According to the ISO 10993-5 standard, if the viability of the cells falls to < 70%, it is considered toxicity[60]. As shown in Figs. 6.a and 6.b, the cell viability was > 80% following the co-cultivation of L929 cells or BMSCs with

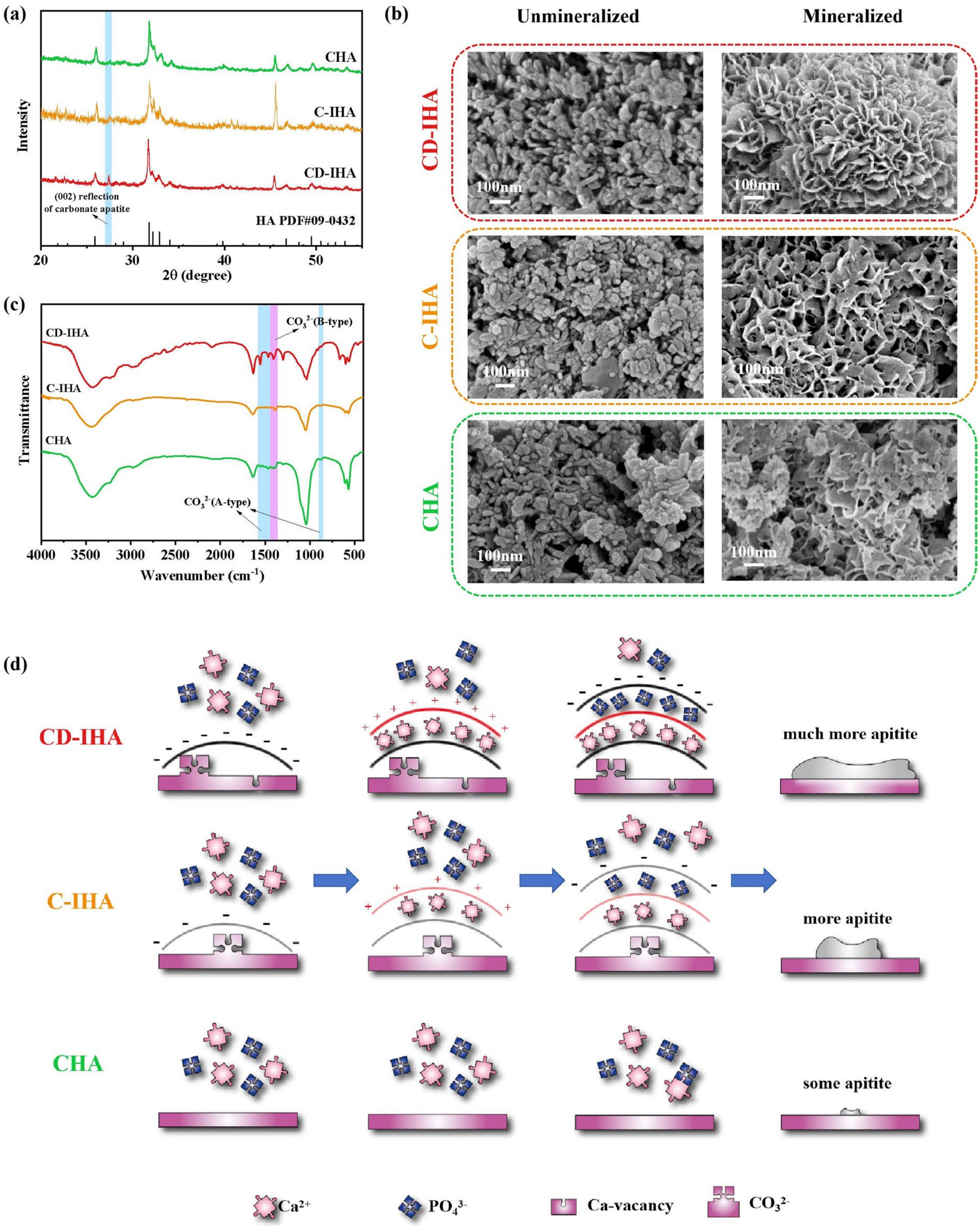

Fig. 5. (a) XRD pattern of CHA, C-IHA and CD-IHA after immersion in SBF; (b) SEM images of CHA, C-IHA and CD-IHA before and after immersion in SBF; (c) FTIR spectra of CHA, C-IHA and CD-IHA after immersion in SBF; and (d) mineralization mechanism of CHA, C-IHA and CD-IHA during immersion in SBF.

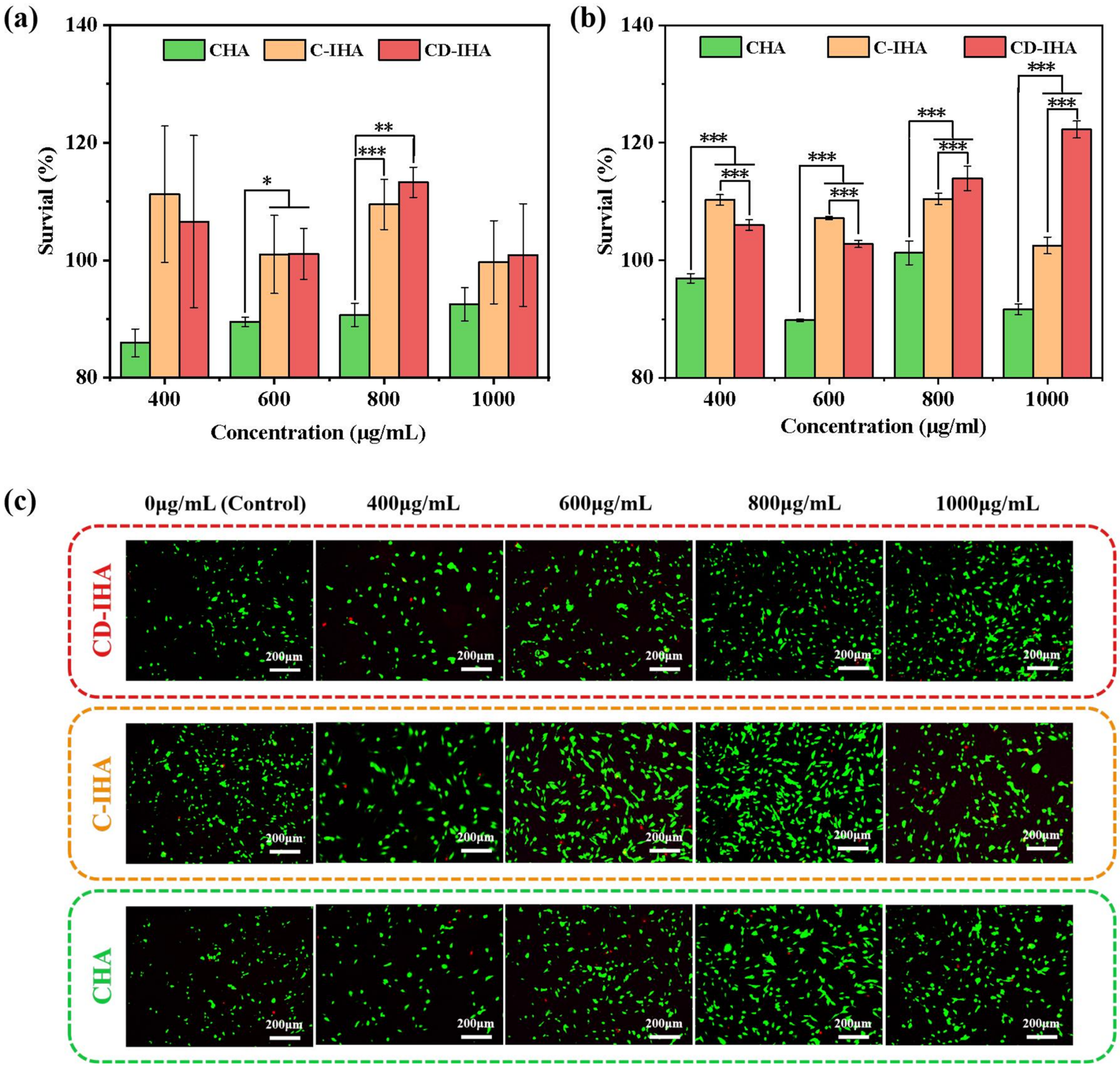

Fig. 6. (a) Cell viability of L929 co-cultured with CHA, C-IHA and CD-IHA at various concentrations; (b) BMSCs co-cultured with CHA, C-IHA and CD-IHA at various concentrations; (c) Calcein-AM/PI staining result of BMSCs co-cultured with CHA, C-IHA and CD-IHA at various concentrations.

CHA or G-IHA at varying concentrations. The live/dead staining results of the BMSCs (Fig. 6.c) also agreed with those of the quantitative evaluation, indicating that both CHA and G-IHA are biocompatible. Consequently, both the CHA and G-IHA exhibited excellent cytocompatibility.

Osteogenic ability in vitro

Bone grafts are more commonly used in situations similar to a suspension, that is, where the particles are surrounded by body fluid at the defect site in vivo, rather than extracts[61]. Consequently, BMSCs were co-cultured with the suspension in this study to evaluate the osteogenic ability of the samples.

ALP is often used as an early stage marker of osteogenesis[62]. This is shown in Fig. 7.a and 7.b, where it could be seen that the ALP activity in CD-IHA and C-IHA reached 58% and 49%, respectively, which was significantly higher than that in CHA (37%, $^{**}p < 0.01$). Additionally, the CD-IHA group exhibited significantly higher ALP activity than the C-IHA group ($^{**}\ p < 0.01$; Figs. 7.a and 7.b). ARS is a late-stage marker of extracellular matrix mineralization[62]. After 14 days of co-cultivation, ARS activity in CD-IHA and C-IHA reached 61% and 39%, respectively, which was significantly higher than that in CHA (27%, $^{***}p < 0.001$ for CD-IHA and $^{**}p < 0.01$ for C-IHA) (Fig. 7.a and c). Furthermore, the CD-IHA group exhibited significantly higher ARS activity than the C-IHA group ($^{***}\ P < 0.001$; Fig. 7.a and c). These results indicate that the suspension of imperfect hydroxyapatite

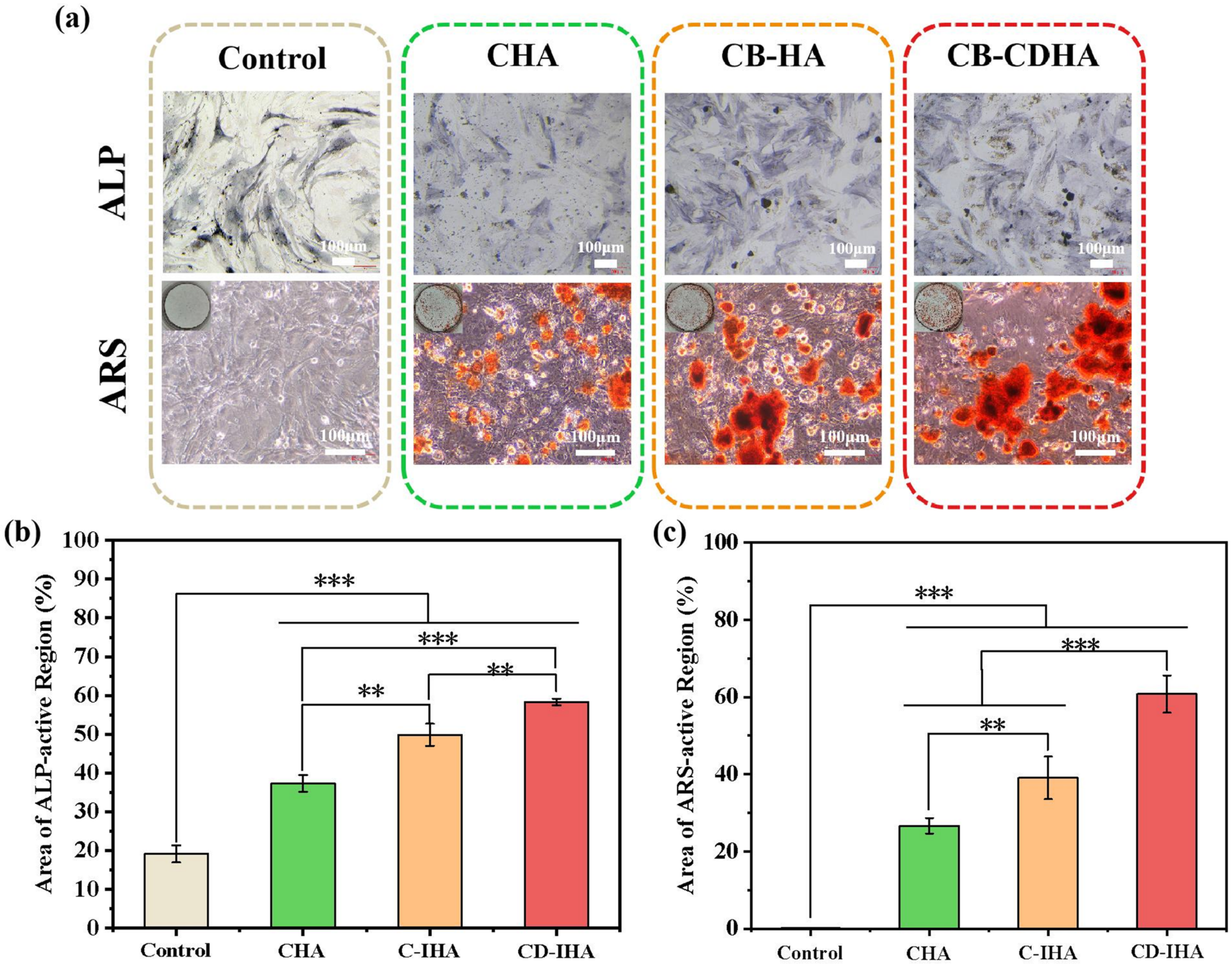

Fig. 7. (a) ALP and ARS staining image of CHA, C-IHA, CD-IHA, and control group; (b) area of ALP-active region of CHA, C-IHA, CD-IHA, and control group; (c) area of ARS-active region of CHA, C-IHA, CD-IHA, and control group.

provides a more favorable environment for osteoblastic differentiation and CaP mineralization in BMSCs[28,63,64]. According to related researches, negative surface of apatite has a higher binding affinity to calcium ions and is capable of enriching them[47]. As a result, G-IHA can facilitate the proliferation and differentiation of osteoblasts via improved ion exchange and interaction, thereby stimulating the subsequent bone formation process[41,47,65].

Ion doping, crystal structure manipulation, and surface affinity modification were proposed as the main methods for enhancing the osteogenic properties of hydroxyapatite[66–68]. The present study effectively obtains negatively charged G-IHA from golden pomfret bone, which possesses an intrinsic crystal defect that includes calcium deficiency and carbonate substitution. Without surface modification, G-IHA increases the osteogenic activity using its crystal structure. Here, we provide a new method for the synthesis of imperfect hydroxyapatite which can be potentially used in bone regeneration.

Conclusion

In this study, the degradation, mineralization, and osteogenic abilities of golden pomfret bone-derived imperfect hydroxyapatite bioceramics (G-IHA) obtained from golden pomfret using a two-step calcination-hydrothermal method were investigated. In particular, carbonate substitution and Ca vacancies resulted in a negatively charged surface on the G-IHA. The negatively charged surface of the HA structure, facilitating the cation exchange and interaction, endowed it with superior degradation, mineralization, and osteogenic properties (Fig. 8). Consequently, G-IHA are likely to become novel and widely used bone graft materials, benefiting > 450 million patients with bone fractures worldwide.

Future research should focus on the production of injectable materials that can sustainably release G-IHA. Thus, G-IHA can implant to the fractures non-invasively and induce osteogenesis on their surface. In vivo investigations will be conducted in the future using different damage models of bone fractures to further verify the biological safety and clinical efficacy of G-IHA.

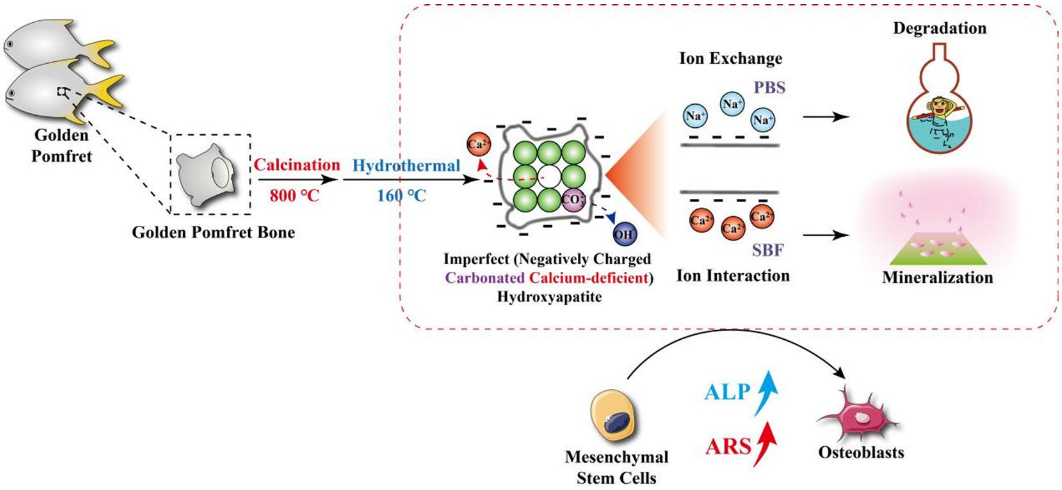

Fig. 8. Illustration of the preparation method and action mode for golden pomfret derived hydroxyapatite.

Data availability

The data that support the findings of this study are available from the corresponding author upon reasonable request.

Received: 5 March 2025; Accepted: 5 June 2025

References

1. Global, G. B. D. Regional, and National burden of bone fractures in 204 countries and territories, 1990–2019: a systematic analysis from the global burden of disease study 2019. *Lancet Health Longev.* **2**, e580–e592 (2021).
2. El-Rashidy, A. A., Roether, J. A., Harhaus, L., Kneser, U. & Boccaccini, A. R. Regenerating bone with bioactive glass scaffolds: a review of in vivo studies in bone defect models. *Acta Biomater.* **62**, 1–28 (2017).
3. Maleki-Ghaleh, H. et al. Antibacterial and cellular behaviors of novel Zinc-Doped hydroxyapatite/graphene nanocomposite for bone tissue engineering. *Int. J. Mol. Sci.* **22**, 9564 (2021).
4. Li, X. et al. Stabilization of Ca-Deficient hydroxyapatite in biphasic calcium phosphate ceramics by adding alginate to enhance their biological performances. *J. Mat. Chem. B*. **6**, 84–97 (2018).
5. Sun, Y., Wang, Y., Ji, C., Ma, J. & He, B. The impact of hydroxyapatite crystal structures and protein interactions on bone's mechanical properties. *Sci. Rep.* **14**, 7412 (2024).
6. Von Euw, S. et al. Bone mineral: new insights into its chemical composition. *Sci. Rep.* **9**, 7489 (2019).
7. Cazalbou, S. et al. Ion exchanges in apatites for biomedical applications. *J. Mater. Sci. Mater. Med.* **2005**, 405–409 (2005).
8. Neuman, W. F. & Mulryan, B. J The surface chemistry of bone. IV. Further data on recrystallization. *J. Biol. Chem.* **193**, 237–241 (1951).
9. Zhang, L. et al. Physicochemical and cytological properties of poorly crystalline Calcium-Deficient hydroxyapatite with different ca/p ratios. *Ceram. Int.* **48**, 24765–24776 (2022).
10. Bulina, N. V. et al. Substituted hydroxyapatite and Β-Tricalcium phosphate as osteogenesis enhancers. *Ceram. Int.* **50**, 33258–33269 (2024).
11. Ishikawa, K. Bone substitute fabrication based on Dissolution-Precipitation reactions. *Materials* **3**, 1138–1155 (2010).
12. Hasegawa, M., Doi, Y. & Uchida, A. Cell-Mediated bioresorption of sintered carbonate apatite in rabbits. *J. Bone Joint Surg. Br.* **85**, 142–147 (2003).
13. Ishikawa, K. et al. Physical and histological comparison of hydroxyapatite, carbonate apatite, and Β-Tricalcium phosphate bone substitutes. *Materials* **11**, 1993 (2018).
14. Duta, L., Dorcioman, G. & Grumezescu, V. A. Review on biphasic calcium phosphate materials derived from fish discards. *Nanomaterials* **11**, 2856 (2021).
15. Borciani, G. et al. Marine biological waste as a source of hydroxyapatite for bone tissue engineering applications. *Ceram. Int.* **49**, 1572–1584 (2023).
16. Shi, P. et al. Characterization of natural hydroxyapatite originated from fish bone and its biocompatibility with osteoblasts. *Mater. Sci. Eng. C*. **90**, 706–712 (2018).
17. Deng, K. et al. HA/Β-TCP biphasic calcium phosphate ceramics derived from butterfish bones loaded with bone marrow mesenchymal stem cells promote osteogenesis. *Front. Mater.* **9**, 748 (2022).
18. Xiong, T. et al. Insights into nutrition, flavor and edible quality changes of golden pomfret (Trachinotus Ovatus) fillets prepared by different cooking methods. *Front. Nutr.* **10**, 423 (2023).
19. Li, M. et al. Dietary supplementation with N-3 high unsaturated fatty acids decreases serum lipid levels and improves flesh quality in the marine teleost golden Pompano Trachinotus Ovatus. *Aquaculture* **516**, 734632 (2020).
20. Yu, G., Luo, Y. & Deng, R. Automatic segmentation of golden pomfret based on fusion of Multi-Head Self-Attention and Channel-Attention mechanism. *Comput. Electron. Agric.* **202**, 107369 (2022).
21. Lou, X. et al. Changes in texture, rheology and volatile compounds of golden pomfret sticks inoculated with Shewanella Baltica during spoilage. *Food Chem.* **404**, 134616 (2023).
22. Qiu, Y. et al. Elucidating the mechanism underlying volatile and Non-Volatile compound development related to microbial amino acid metabolism during golden pomfret (Trachinotus Ovatus) fermentation. *Food Res. Int.* **162**, 112095 (2022).
23. Oyane, A. et al. Formation and growth of clusters in conventional and new kinds of simulated body fluids. *J. Biomed. Mater. Res. A*. **64A**, 339–348 (2003).
24. Rietveld, H. M. A profile refinement method for nuclear and magnetic structures. *J. Appl. Crystallogr.* **2**, 65–71 (1969).

25. Person, A. et al. Early diagenetic evolution of bone phosphate; an X-Ray diffractometry analysis. *J. Archaeol. Sci.* **22**, 211–221 (1995).
26. Liu, H. et al. Ca2+/PH-Triggered gelation of Pickering emulsion in vitro digestion: visualization and Sustained-Release performance. *Food Hydrocoll.* **140**, 108583 (2023).
27. Carvajal-Agudelo, J. D., McNeil, A. & Franz-Odendaal, T. A. Effects of simulated microgravity and vibration on osteoblast and osteoclast activity in cultured zebrafish scales. *Life Sci. Space Res.* **38**, 39–45 (2023).
28. Cao, X. et al. Magnesium-Rich calcium phosphate derived from Tilapia bone has superior osteogenic potential. *J Funct. Biomater* **14**, 4123 (2023).
29. Wang, T., Watanabe, K., Hamada, N. & Tani-Ishii, N. Role of MAPKs in TGF-B1-Induced maturation and mineralization in human Osteoblast-Like cells. *J. Oral Biosci.* **66**, 61–67 (2024).
30. Goto, T. & Sasaki, K. Synthesis of morphologically controlled hydroxyapatite from fish bone by Urea-Assisted hydrothermal treatment and its Sr2 + Sorption capacity. *Powder Technol.* **292**, 314–322 (2016).
31. Kashyap, S. J., Sankannavar, R. & Madhu, G. M. Hydroxyapatite nanoparticles synthesized with a wide range of ca/p molar ratios and their structural, optical, and dielectric characterization. *J. Korean Ceram. Soc.* **59**, 846–858 (2022).
32. Zhang, X. et al. Temperature dependent vacancy formation energy of metallic materials. *Phys. B: Condens. Matter*. **584**, 412071 (2020).
33. Tkalcec, E., Popovic, J., Orlic, S., Milardovic, S. & Ivankovic, H. Hydrothermal synthesis and thermal evolution of Carbonate-Fluorhydroxyapatite scaffold from cuttlefish bones. *Mater. Sci. Eng.: C* 578–586 (2014).
34. Sudhakar, M. S. et al. Exploring fish Scale-Derived hydroxyapatite doped with NaCl for enhanced bone tissue regeneration. *Mater. Int.* **6**, 19 (2024).
35. Nam, P. V., Hoa, N. V. & Trung, T. S. Properties of hydroxyapatites prepared from different fish bones: a comparative study. *Ceram. Int.* **45**, 20141–20147 (2019).
36. Boudreau, S. et al. Transforming waste fish bones into nanoparticles with ultrasound and aqueous organic acids. *RSC Sustain.* (2025).
37. Shu, C., Yanwei, W., Hong, L., Zhengzheng, P. & Kangde, Y. Synthesis of carbonated hydroxyapatite nanofibers by mechanochemical methods. *Ceram. Int.* **31**, 135–138 (2005).
38. Murugan, R., Panduranga Rao, K. & Sampath Kumar, T. S. Microwave synthesis of bioresorbable carbonated hydroxyapatite using Goniopora. *Key Eng. Mater.* **240–242**, 51–54 (2003).
39. Yasukawa, A., Kandori, K. & Ishikawa, T. TPD-TG-MS study of carbonate calcium hydroxyapatite particles. *Calcif Tissue Int.* **72**, 243–250 (2003).
40. Bee, S. & Hamid, Z. A. A. Characterization of chicken bone Waste-Derived hydroxyapatite and its functionality on Chitosan membrane for guided bone regeneration. *Compos. Part. B: Eng.* **163**, 562–573 (2019).
41. Bodhak, S., Bose, S. & Bandyopadhyay, A. Electrically polarized HAp-Coated ti: in vitro bone Cell–Material interactions. *Acta Biomater.* **6**, 641–651 (2010).
42. Liu, S. et al. Maintaining sidedness and fluidity in cell membrane coatings supported on Nano-Particulate and planar surfaces. *Bioact Mater.* **32**, 344–355 (2024).
43. Skwarek, E. & Janusz, W. The influence of carbonate ions on the structure of the electrical double layer at the interface of hydroxyapatite/electrolyte solution. *Mater. Sci.* **22**, 145 (2016).
44. de Leeuw, N. H., Bowe, J. R. & Rabone, J. A. L. A computational investigation of stoichiometric and Calcium-Deficient Oxy- and Hydroxy-Apatites. *Faraday Discuss.* **134**, 195–214 (2007).
45. Dorozhkin, S. Calcium orthophosphates in nature, biology and medicine. *Materials* **2**, 399–498 (2009).
46. Wang, Y. et al. Degradation mechanism of Lead-Vanado-Iodoapatite in NaCl solution. *Corros. Sci.* **172**, 108720 (2020).
47. Ohgaki, M., Kizuki, T., Katsura, M. & Yamashita, K. Manipulation of selective cell adhesion and growth by surface charges of electrically polarized hydroxyapatite. *J. Biomed. Mater. Res.* **57**, 366–373 (2001).
48. Porter, A. E., Patel, N., Skepper, J. N., Best, S. M. & Bonfield, W. Comparison of in vivo dissolution processes in hydroxyapatite and Silicon-Substituted hydroxyapatite bioceramics. *Biomaterials* **24**, 4609–4620 (2003).
49. Zhu, H. et al. Enhancement of hydroxyapatite dissolution through structure modification by Krypton ion irradiation. *J. Mater. Sci. Technol.* **38**, 148–158 (2020).
50. Zhang, Y. et al. Expression, purification, and refolding of a Recombinant human bone morphogenetic protein 2 in vitro. *Protein Expr Purif.* **75**, 155–160 (2011).
51. Maazouz, Y., Chizzola, G., Döbelin, N. & Bohner, M. Cell-Free, quantitative mineralization measurements as a proxy to identify osteoinductive bone graft substitutes. *Biomaterials* **275**, 120912 (2021).
52. Ma, B. et al. Preparation and properties of biomimetic Hydroxyapatite-Based nanocomposite utilizing bamboo Fiber. *Cellulose* **27**, 2069–2083 (2020).
53. Liu, Y., Thibodeaux, D., Gamble, G., Bauer, P. & VanDerveer, D. Comparative investigation of fourier transform infrared (FT-IR) spectroscopy and X-Ray diffraction (XRD) in the determination of cotton Fiber crystallinity. *Appl. Spectrosc.* **66**, 983–986 (2012).
54. Murphy, W. L. & Mooney, D. J. Bioinspired growth of crystalline carbonate apatite on biodegradable polymer substrata. *J. Am. Chem. Soc.* **124**, 1910–1917 (2002).
55. Ait Hamdan, Y., Elouali, S., Oudadesse, H., Lefeuvre, B. & Rhazi, M. Exploring the potential of chitosan/aragonite biocomposite derived from cuttlebone waste: elaboration, physicochemical properties and in vitro bioactivity. *Int. J. Biol. Macromol.* **267**, 131554 (2024).
56. Bollmeyer, M. M., Carney, M. C. & Yoder, C. H. A-Type carbonate in strontium phosphate apatites. *Am. Mineral.* **104**, 438–446 (2019).
57. Yoder, C. H., Landes, N. T., Tran, L. K., Smith, A. K. & Pasteris, J. D. The relative stabilities of a- and B-Type carbonate substitution in apatites synthesized in aqueous solution. *Mineral. Mag.* **80**, 977–983 (2016).
58. Rey, C. et al. The carbonate environment in bone mineral: a Resolution-Enhanced fourier transform infrared spectroscopy study. *Calcif Tissue Int.* **45**, 157–164 (1989).
59. Koons, G. L., Diba, M. & Mikos, A. G. Materials design for Bone-Tissue engineering. *Nat. Reviews Mater.* **5**, 584–603 (2020).
60. Kolekar, T. V., Bandgar, S. S., Yadav, H. M., Kim, D. & Magalad, V. T. Hemolytic and biological assessment of Lithium substituted hydroxyapatite nanoparticles for L929 and Hela cervical Cancer cells. *Inorg. Chem. Commun.* **137**, 109172 (2022).
61. Zhang, M. et al. Research advances of nanomaterials for the acceleration of fracture healing. *Bioact Mater.* **31**, 368–394 (2024).
62. Qureshi, A. T. et al. *Human Adipose-Derived Stromal/Stem Cell Isolation, Culture, and Osteogenic Differentiation* 67–88 (Elsevier Science & Technology, 2014).
63. Pang, B. et al. Cuttlefish Bone-Derived calcium phosphate bioceramics have enhanced osteogenic properties. *J. Funct. Biomater.* **15**, 212 (2024).
64. Wang, J. et al. Ultrathin WOx nanoribbons with moderate ROS clearance and antibacterial abilities efficiently induce M2 macrophage polarization for diabetic bone defect repair. *Adv Funct. Mater.* (2023).
65. Chai, Y. C. et al. Current views on calcium phosphate osteogenicity and the translation into effective bone regeneration strategies. *Acta Biomater.* **8**, 3876–3887 (2012).
66. Murugan, E., Akshata, C. R., Ilangovan, R. & Mohan, M. Evaluation of quaternization effect on Chitosan-HAP composite for bone tissue engineering application. *Colloids Surf., B.* **218**, 112767 (2022).

67. Liu, C. et al. Exploring the potential of Hydroxyapatite-Based materials in biomedicine: a comprehensive review. *Mater. Sci. Engineering: R: Rep.* **161**, 100870 (2024).
68. Salam, N. & Gibson, I. R. Lithium ion doped carbonated hydroxyapatite compositions: synthesis, physicochemical characterisation and effect on osteogenic response in vitro. *Biomaterials Adv.* **140**, 213068 (2022).
69. Momma, K. & Izumi, F. *VESTA 3* for Three-Dimensional visualization of crystal, volumetric and morphology data. *J. Appl. Crystallogr.* **44**, 1272–1276 (2011).

Acknowledgements

Z.C. et al. acknowledges Zhongkebaice (www.zkbaice.cn) for acquiring SEM and DTG, acknowledges Ceshigo Research Service (www.ceshigo.com) for acquiring ALP and ARS staining, acknowledges Servier Smart Art (smart.servier.com) for acquiring graphics of adhesion proteins, BMSCs and osteoblasts in Fig. 8, acknowledges Editage (www.editage.cn) for English language editing.

Author contributions

Changze Zhang: Investigation and Writing - original draft. Guangchun Zhao: Formal analysis. Xiaorui Wang: Data curation. Mengting Li: Methodology and Writing - review & editing. Zhengmao Li: Data curation. Yixun E: Investigation. Xiaxin Cao: Formal analysis. Maohua Chen: Methodology. Chaozong Liu: Supervision and Project administration. All authors reviewed the manuscript.

Funding

This work was funded by the Natural Science Foundation of China (grant No. 32401110), International Science & Technology Cooperation Program of Hainan Province (grant No. GHYF2022001), Science and Technology Projects in Guangzhou (202201020396), National Natural Science Foundation of China (NO.32360238), Hainan Provincial Natural Science Foundation (No. 524RC479).

Competing interests

The authors declare no competing interests.

Additional information

Correspondence and requests for materials should be addressed to M.L., M.C. or C.L.